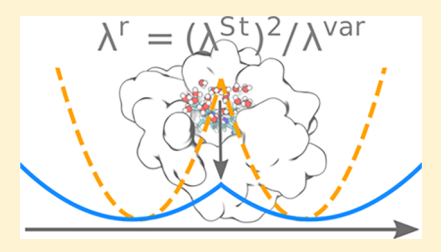
# Polarizability of the Active Site in Enzymatic Catalysis: Cytochrome c

Daniel R. Martin, Mohammadhasan Dinpajooh, and Dmitry V. Matyushov\*, and Dmitry V. Matyushov

<sup>†</sup>Department of Physics and <sup>‡</sup>Department of Physics and School of Molecular Sciences, Arizona State University, P.O. Box 871504, Tempe, Arizona 85287, United States

Supporting Information

**ABSTRACT:** Anisotropic polarizability of the heme in cytochrome c is found to be a major factor in suppressing the activation barrier of protein electron transfer (catalytic effect). Polarizability couples to the electric field of protein and water to enhance fluctuations of the electron-transfer energy gap and the corresponding variance reorganization energy  $\lambda^{\text{var}}$ . The reorganization energy observable by kinetic measurements  $\lambda^{\text{r}} = (\lambda^{\text{St}})^2/\lambda^{\text{var}}$  is composed of  $\lambda^{\text{var}}$  and the Stokes-shift reorganization energy  $\lambda^{\text{St}}$ . It is lowered compared to the usually reported  $\lambda^{\text{St}}$  due to polarizability of the active site leading to  $\lambda^{\text{var}} > \lambda^{\text{St}}$ . The coupling of electrostatic protein-water fluctuations to the polarizable active site is accounted for here by empirical valence-



bond diagonalization of the active-site Hamiltonian along the simulation trajectory. We show that recent simulations employing this technique, which failed to find the effect of polarizability on electron-transfer kinetics, were erroneous in neglecting the diagonal dipole moments in the Hamiltonian matrix and failing to rotate the electric field produced by the protein-water medium into the molecular frame of the active site. We find that anisotropy of the tensor of polarizability difference in the two oxidation states of the heme matches anisotropy of the second-rank tensor constructed from the electric field at the active site. Exposure of the heme to water from only one side carries significant catalytic function, directly leading to the field anisotropy and the corresponding depression of the activation barrier.

# INTRODUCTION

The function of natural enzymes is to lower the activation barrier to catalyze chemical reactions. Redox proteins in energy chains of biology lower barriers for transferring electrons. How this function is achieved is still the matter of active study and debate. This report discusses the coupling of the electronic polarizability of the active site to the proteinwater electrostatics as the mechanism for lowering the activation barrier for protein electron transfer.

The Marcus theory of electron transfer is a general framework for describing electronic transitions driven by Gaussian fluctuations of the medium coupled to the donor and acceptor electronic states. It greatly reduces the complexity of the problem to only two parameters affecting the activation barrier: the reorganization energy  $\lambda$  and the reaction free energy  $\Delta F_0$ , both being free energies depending on the thermodynamic state of the system. The free energy of activation becomes

$$\Delta F^{\dagger} = (\lambda + \Delta F_0)^2 / (4\lambda) \tag{1}$$

For a half reaction studied by electrochemistry,  $^3$   $\Delta F_0 = e\eta$  is replaced with the product of the elementary charge e with the electrode overpotential  $\eta$ . Changing  $\eta$  in the electrochemical experiment, such as cyclic voltammetry, provides access to the reorganization energy  $\lambda$  and the standard reaction rate at  $\eta=0$ . The standard rate constant gives access to  $\lambda$  if the rate pre-exponential factor is known. Since this is mostly not the case, additional information is typically obtained from the Arrhenius

plot of the rate yielding the enthalpy of activation. We first discuss what is known from this type of kinetic data and then turn to numerical simulations of the half reaction of protein electron transfer.

Electrochemistry of proteins immobilized on alkanethiol self-assembled monolayers covering the metal electrode has given evidence of low values of the reorganization energy for electron transfer. These results have confirmed the anticipated catalytic effect by the protein environment.<sup>4</sup> For instance, protein electrochemistry reports  $\lambda \simeq 0.57$  eV for cytochrome c,5,6 0.5 eV for myoglobin,7 and 0.3 eV for azurin.8,9 However, even lower reorganization energies have been reported. 10,11 Further, the analysis of Arrhenius plots mostly yields a good agreement between the enthalpy of activation  $\Delta H^{\dagger}$  and  $\lambda/4$ , <sup>8,9</sup> thus suggesting a weak dependence of the reorganization energy on temperature.7 This result comes in contrast to a much steeper functions  $\lambda(T)$ , which decreases with increasing temperature, found for organic donor-acceptor systems in aqueous and nonaqueous media. 12 We will return to this point below.

Overall, the reorganization energies of protein electron transfer found by electrochemistry are significantly below the common estimates offered by the Marcus theory and, more importantly, by measurements performed with Ru-ligated electron donors attached to the surface of a redox protein.

Received: September 30, 2019 Revised: November 14, 2019 Published: November 17, 2019



<sup>§</sup>Department of Chemistry, University of Pennsylvania, Philadelphia, Pennsylvania 19104, United States

Such measurements give  $\lambda \simeq 0.74$  eV for cytochrome c, <sup>13</sup> in contrast to 0.57 eV from electrochemistry. <sup>5,6</sup> Similarly,  $\lambda \simeq 0.8$  eV was reported for Ru-modified azurins, <sup>4</sup> in contrast to  $\lambda \simeq 0.3$  eV found by electrochemistry. <sup>8,9</sup> Along the same lines,  $\lambda \simeq 0.78$  eV was reported for electron transfer from the disulfide at the surface of azurin produced by pulse radiolysis. <sup>14</sup> In all these cases of intraprotein electron transfer, the reorganization energy is strongly affected by solvation of the electron donor exposed to the aqueous solution and does not directly report on reorganization of the active site. <sup>15</sup> Electrochemistry provides a more direct test of medium reorganization produced by the protein-water environment.

Another troubling disconnect with the reorganization energies measured by electrochemistry comes from atomistic simulations of proteins. Most recent simulations employing nonpolarizable force fields have produced high reorganization energies  $\lambda > 1$  eV, for example, 2.1 eV for [FeFe]-hydrogenase<sup>16</sup> and 1.3–1.6 eV for electron transfer between the bacteriopheophytin and primary quinone cofactors of the photosynthetic bacterial reaction center (at the length of the simulation trajectory). These large reorganization energies come from the protein-water solvent. On the other hand, large reorganization energies ~1.2–1.5 eV recently reported for the DNA repair enzyme photolyase were attributed to structural distortions of the flavin cofactor. In contrast, the internal reorganization energy is small for heme proteins. Before attempting the theory—experiment comparison, we first summarize how the reorganization energies are computed in numerical simulations.

The tunneling configuration for electron transfer is reached when the energy gap between the electronic states of the acceptor and donor taken at the same nuclear configuration is zero. The energy gap  $X = \Delta E$  then becomes the reaction coordinate for electron transfer, with the transition-state configuration at X = 0. If the statistics of X is Gaussian, it is characterized by two statistical moments, the average  $X_i$  =  $\langle \Delta E \rangle_i$  and the variance  $\sigma_i^2 = \langle (\delta X)^2 \rangle_i$ , where i = Ox, Red specifies two oxidation states of the half reaction. One in principle needs four parameters to characterize the Gaussian fluctuations in the two oxidation states, but a significant simplification is achieved in the Marcus theory assuming  $\sigma_{Ox}^2$  =  $\sigma_{\text{Red}}^{2} = 2k_{\text{B}}T\lambda$ . When this requirement is combined with the canonical Gibbs distribution of statistical configurations, one additionally obtains  $|X_1 - X_2| = 2\lambda$  and  $(X_1 + X_2)/2 = \Delta F_0$ . Four statistical parameters are reduced to only two required in

The definition of the reaction coordinate in terms of the energy gap provides a numerical algorithm to calculate the experimentally observable  $\lambda$  and  $\Delta F_0$  in eq 1.  $^{21,22}$  At the same time, one gets the consistency test between two routes to the reorganization energy: one can either take the Stokes-shift reorganization energy  $\lambda_i^{\rm St} = \frac{1}{2}|X_1 - X_2|$  or the variance reorganization energy  $\lambda_i^{\rm var} = (\beta/2)\langle(\delta X)^2\rangle_i$ . The Marcus theory stipulates  $\lambda_i^{\rm St} = \lambda_{\rm Red}^{\rm var} = \lambda_{\rm Ox}^{\rm var}$ . Since  $\lambda_i^{\rm St}$ , being the combination of two first-order statistical moments, converges much faster than  $\lambda_i^{\rm var}$ , most numerical studies report  $\lambda_i^{\rm St}$  and then construct the activation barrier based on  $\lambda = \lambda_i^{\rm St}$  in eq 1.

The Gaussian statistics of X is realized for a specific model of coupling between the donor and acceptor electronic states to the typically Gaussian thermal bath. A linear coupling to the medium converts the Gaussian fluctuations of the medium into Gaussian fluctuations of the donor—acceptor energy gap. Any

nonlinear coupling to the bath leads to non-Gaussian fluctuations of the energy gap. Such a nonlinear coupling to the electrostatic field of the medium is, for instance, realized for polarizable solutes.<sup>23</sup> If one assumes that the active site of the protein carries the charge  $Q_i$  and the polarizability  $\alpha_i$  (second-rank tensor), the solvent-induced shift of the electronic energy level becomes

$$\Delta E_{s} = \Delta Q \phi_{b} - \frac{1}{2} \mathbf{E}_{b} \cdot \Delta \boldsymbol{\alpha} \cdot \mathbf{E}_{b}$$
(2)

where  $\Delta Q = Q_{\rm Red} - Q_{\rm Ox} = -e$  and  $\Delta \alpha = \alpha_{\rm Red} - \alpha_{\rm Ox}$ . Further,  $\phi_{\rm b}$  is the fluctuating electrostatic potential at the active site and  $E_{\rm b}$  is the fluctuating vector of the electric field. If the polarizability does not change in electron transfer,  $\Delta \alpha = 0$  and one arrives at the linear coupling of the energy gap to the Gaussian stochastic variable  $\phi_{\rm b}$ . This limit recovers the standard Marcus theory. If, on the other hand,  $\Delta \alpha \neq 0$ , the energy gap  $\Delta E_{\rm s}$  depends quadratically on the Gaussian field  $E_{\rm b}$  and its statistics is non-Gaussian. The consequence is that there are two different reorganization energies  $\lambda_i^{\rm var}$  in the two oxidation states and  $\lambda^{\rm St} \neq \lambda_i^{\rm var}$ . The deviation from the Gaussian statistics can be quantified by the parameter<sup>2-4</sup>

$$\kappa_{\rm G} = \lambda^{\rm var}/\lambda^{\rm St}, \quad \lambda^{\rm var} = \frac{1}{2}(\lambda_{\rm Ox}^{\rm var} + \lambda_{\rm Red}^{\rm var})$$
(3)

with  $\kappa_G = 1$  for the Marcus theory.

Recent progress in parallel simulations of biomolecules has allowed one to sample the complete distribution of the electron-transfer energy gap and to test the requirement of  $\kappa_G$ = 1 stipulated by the Marcus theory. Somewhat surprisingly, it was found that  $\kappa_G$  extracted from simulations involving nonpolarizable active sites can reach large values  $\kappa_G \simeq 2-5$  well beyond simulation uncertainties. Since nonlinear coupling between the active site and the protein-water medium is not involved in these simulations, the only requirement that can be broken to allow this to happen is the assumption of the Gibbs canonical ensemble. It was, therefore, suggested that insufficient sampling, that is, nonergodicity of the system, contributes to  $\kappa_G > 1$ . This result was confirmed for a number of proteins: plastocyanin,<sup>25</sup> bacterial reaction center,<sup>17,26</sup> green fluorescent protein,<sup>27</sup> bacterial bc<sub>1</sub> complex,<sup>28,29</sup> and bacterial complex I.30 One has to stress that long simulations, in the range of hundreds of nanoseconds, are required to achieve sufficient statistics for  $\lambda^{\text{var}}$  even for a small globular protein; 15 us simulations were employed for the membrane-bound bc<sub>1</sub> complex.<sup>29</sup> Comparison to experiment was possible in most of these studies, and the condition  $\kappa_{\rm G} > 1$  was very essential to bring the simulation results in agreement with experimental kinetic and electrochemical data. The reorganization energy  $\lambda^{St}$ was too large to achieve theory-experiment agreement, but it was recognized that  $\lambda$  in eq 1 should be replaced with the "reaction" reorganization energy  $\lambda^{r}$  composed of  $\lambda^{St}$  and  $\lambda^{var}$ 

$$\lambda^{\rm r} = (\lambda^{\rm St})^2 / \lambda^{\rm var} \tag{4}$$

This result comes from considering crossing of two parabolas with different curvatures. Since  $\lambda^{\rm St} < \lambda^{\rm var}$  was consistently found in simulations,  $\lambda^{\rm r} < \lambda^{\rm St}$  produced good agreement between simulations and kinetic rate measurements.

A somewhat different situation was found for the cytochrome c heme protein. Standard simulations involving the Coulomb interaction of the charges in the active site with the electrostatic potential of the bath,  $\Delta Q \phi_b \rightarrow \sum_j \Delta q_j \phi_{bj}$  in eq 2, produced  $\lambda^{\rm St} \simeq 1.26 \ {\rm eV}^{32}$  and  $\kappa_{\rm G} \simeq 1.3$ , in accordance with

other simulations.<sup>33</sup> Here,  $\Delta q_j = q_{j, \text{Red}} - q_{j, \text{Ox}}$  are the changes in atomic charges of the active site coupled with the site electrostatic potentials  $\phi_{\mathrm{bj}}$ . Since the experimental  $\lambda^{\mathrm{r}}$  is about half of the simulated  $\lambda^{5}$ , the possibility of a polarizable active site was considered.<sup>32</sup> It was indeed found that applying Warshel's valence-bond<sup>33–35</sup> approach to the heme of cytochrome c brought the results of calculations in accordance with experiment. We obtained, by interpolating through a number of temperatures,  $^{36}$   $\lambda^{\text{St}} = 1.26$  eV,  $\lambda^{\text{var}}_{\text{Ox}} = 2.90$  eV, and  $\lambda^{\text{var}}_{\text{Red}} = 2.81$  eV. From these values, the mean variance reorganization energy  $\lambda^{\text{var}} = 2.86 \text{ eV}$  is given by eq 3 and  $\lambda^{\text{r}}$ = 0.56 eV follows from eq 4. This value agrees with the experimental result of  $0.58 \pm 0.04$  eV.<sup>5,6</sup> Since the polarizability is a parameter slowly converging with the number of quantum states, a large number of excited states M = 100calculated in ZINDO/S approximation were required to converge the polarizability of the heme to  $\alpha_{Ox} = 23 \text{ Å}^3$  and  $\alpha_{\rm Red} = 54 \, \text{Å}^3$ , where  $\alpha_i = (1/3) \text{Tr}[\alpha_i]$  is the isotropic trace of the anisotropic polarizability tensor.

In a recent paper,<sup>37</sup> Blumberger and co-workers reported long,  $\sim$ 250 ns, simulations of the cytochrome c half reaction applying a number of simulation protocols. Their results can be briefly summarized by two statements: (i) they could not reproduce an increase of the reorganization energy  $\lambda^{\mathrm{var}}$  and  $\kappa_{\mathrm{G}}$ > 1 when the polarizability of the active site was introduced in terms of the empirical valence-bond method and (ii) they found, consistently with the previous reports from the same group,<sup>38</sup> that introducing polarizable force fields lowers  $\lambda^{St}$  to a value comparable with the experimental reports. Their conclusion was that polarizability of the active site does not need to be involved to achieve an agreement with experiment in the framework of the standard Marcus model. This report reanalyzes their data and shows that the omission of a number of key factors in the calculation algorithm resulted in erroneous conclusions. We also show that anisotropic polarizability of the active site strongly affects the kinetics of electron transfer in cytochrome c becoming a key factor of the catalytic effect achieved by this redox enzyme.

Previous simulations of proteins showing  $\kappa_{\rm G} > 1$  have strongly suggested that proteins achieve depression of the activation barrier, that is, the catalytic effect, by producing conditions for incomplete (nonergodic) sampling of their configuration space.<sup>31</sup> The activation barrier at  $\Delta F_0 = 0$  becomes

$$\Delta F^{\dagger} = \frac{1}{\kappa_{\rm G}} \frac{\lambda^{\rm St}}{4} \tag{5}$$

The protein in regard to electron transfer behaves as a glassy system  $^{39-42}$  in which the time  $\tau_{\rm sam}$  required to sample the configuration space far exceeds the time of observation, which is the reaction time  $\tau_{\rm r} \simeq k_{\rm ET}^{-1}; \, k_{\rm ET}$  is the rate constant of electron transfer. Single molecule measurements have reported significant protein dynamics on the millisecond timescale  $^{43,44}$  and, from this perspective, an electron-transfer reaction occurring on a microsecond timescale is a nonergodic event.

Nonergodic sampling responsible for the catalytic effect of proteins<sup>31</sup> is quite distinct from the commonly applied Pauling's concept of stabilizing the activated state by natural enzymes.<sup>1</sup> Quoting from Gray and Winkler:<sup>4</sup> "The reorganization energy for electron self-exchange in Cu(phen)<sub>2</sub><sup>2+/+</sup> is 2.4 eV; the value for Cu(II/I) in *Pseudomonas aeruginosa* azurin is 0.7 eV. The 1.7 eV reduction in  $\lambda$  reflects the transition-state

stabilization imposed by the azurin fold." The transition-state stabilization advocated in this quote is the application of Pauling's idea to redox proteins. This idea in fact clashes with the conceptual framework of the Marcus theory, which stipulates that only equilibrium properties (first and second statistical moments) and not nonequlibrium stabilization of the activated state are what needed to determine the activation barrier. Further, the core of a typical redox protein, such as cytochrome c, is quite rigid and densely packed, with little structural change induced by altering its redox state.<sup>45</sup>-Stabilization of the active site by some specific prearrangement of charges is hardly conceivable for electron-transfer catalysis: any static field within the protein (which can be quite strong<sup>49</sup>) cancels from both  $\lambda^{\text{St}}$  and  $\lambda^{\text{var}}$  and should not affect reactions with  $\Delta F_0 = 0$ . On the contrary, breaking the rules of sampling imposed by the Gibbs ensemble is a successful alternative strategy for achieving the catalytic effect.

Cytochrome c is an important study case because non-ergodic sampling is not achieved for this protein, at least with the present simulation evidence. Since the reported reorganization energy of cytochrome c is on par with other proteins, an alternative mechanism of lowering the barrier must have been realized. It appears that polarizability of the active site is what provides the required  $\kappa_G \simeq 2.3$ , although this is not the only conceivable mechanism. For instance, wetting of the active site  $^{33,50}$  caused by electron transfer was also found to lead to  $\kappa_G > 1$  for another small redox protein, ferredoxin. Returning to the question of specificity of the protein fold, we find that it allows specific anisotropy of near-equilibrium electrostatic fluctuations but not a specific stabilization of the activated state.

In this study, we reanalyze the results of simulations of cytochrome c with a polarizable active site. The utilize both the empirical valence-bond approach to calculate the reorganization parameters and a simplified description in terms of the linear anisotropic polarizability of the active site. This latter approach is less computationally demanding and produces results qualitatively consistent with the full diagonalization of the active-site Hamiltonian matrix along the simulation trajectory. We find that anisotropy of the polarizability matrix couples with anisotropy of the medium electric field to enhance the reorganization energy  $\lambda^{\rm var}$ .

## RESULTS

The electron-transfer energy gap along the simulation trajectory is defined by taking the difference of energies of Red and Ox states at each nuclear configuration of the system. These energies are specified differently in the empirical valence-bond approach and in the simplified model involving the gas-phase dipolar polarizability given by eq 2. In the former case, one gets

$$X = E_{\rm g}^{\rm Red} - E_{\rm g}^{\rm Ox} \tag{6}$$

where  $E_{\rm g}^i$  are the ground-state energies obtained by diagonalizing the  $M \times M$  Hamiltonian matrix at each configuration  $(\phi_{\rm b}, E_{\rm b})$  along the trajectory. The Hamiltonian matrix is given in the form

$$H_{jk}^{i} = (E_{j}^{i} + Q^{i}\phi_{b})\delta_{jk} - \mu_{jk}^{i} \cdot \mathbf{E}_{b}$$
(7)

Here,  $Q^i$  is the total charge of the quantum center for which ZINDO/S calculations were performed.<sup>32</sup> Further,  $\mu_{jk}^i$  at  $j \neq k$  are the transition dipoles between states j = 1, ..., M and k = 1,

..., M carrying the energies  $E^i_j$  and  $E^i_k$ , where i=Ox, Red. The diagonal elements of the matrix  $\mu^i_{kk}$  are the dipole moments in the states k=1,...,M. The terms  $-\mu^i_{kk} \cdot E_b$  in the Hamiltonian matrix account for the interaction of the dipole moment of the heme with the electric field of the protein-water medium, while the term  $Q^i\phi_b$  accounts for the interaction of the total charge of the heme with the electrostatic potential. The model used here truncates all higher multipoles starting with the quadrupole moment of the heme. The total charge of the quantum center is  $Q^{Ox}=-1$  in the Ox state and  $Q^{Red}=-2$  in the Red state in our calculations. The vacuum polarizabilities of the quantum center based on these calculations are listed in Table 1.

Table 1. Eigenvalues of the Polarizability Matrix  $\alpha_k$  (k=1, 2, 3), Isotropic Polarizability  $\alpha=(1/3)\mathrm{Tr}[\alpha]$  (ų), and the Polarizability Anisotropy  $\gamma$  (ų),  $\gamma^2=(1/2)(3\mathrm{Tr}[\alpha^2]-\mathrm{Tr}[\alpha]^2)$ 

state	$lpha_1$	$\alpha_2$	$\alpha_3$	α	γ
Ox	37.4	31.7	1.1	23.4	33.9
Red	81.2	77.6	3.7	54.2	75.8

The polarizability tensors  $\alpha_i$  are linear dipolar polarizabilities calculated from transition dipoles and energy differences between vacuum states j and k. On the other hand, the ground-state energies  $E_{g}^{i}$  incorporate powers of the field  $E_{b}$  up to the Mth order. This algorithm, based on diagonalizing the Hamiltonian matrix in eq 7, is, therefore, more advanced than the linear polarizability model and includes a set of higherorder polarizabilities produced by expanding  $E_{\sigma}^{i}$  in powers of  $\mathbf{E}_{\rm b}$ . In other words, the polarizability  $\boldsymbol{\alpha}_i(\mathbf{E}_{\rm b})$  calculated from  $E_{\rm g}^i$ is affected by fluctuations of the electric field not included in the vacuum polarizability  $\alpha_i$ . Based on these arguments, there is no reason to expect an exact match between the empirical valence-bond diagonalization and the linear model given by eq 2. However, it provides a useful benchmark for the calculations since polarizability of the active site enters calculation in an analytical form and does not rely on a specific set of transition dipoles. In this model, the energy gap is linear in the medium electrostatic potential and is quadratic in the medium field. Correspondingly, the coordinate *X* is a sum of its average value plus the fluctuation

$$\delta X = -e\delta\phi_{b} - \frac{1}{2}\Delta\alpha : [\mathbf{F}_{b} - \langle \mathbf{F}_{b} \rangle_{i}]$$
(8)

where  $\delta\phi_{\rm b}=\phi_{\rm b}-\langle\phi_{\rm b}\rangle_i$  and  $F_{\rm b}^{\alpha\beta}=E_{\rm b}^{\alpha}E_{\rm b}^{\beta},~\alpha,~\beta=x,~y,~z$  is the second-rank electric field tensor, and the colon indicates the tensor contraction.

Calculating the variance of  $\delta X$  along the simulation trajectory provides us with a direct estimate of the variance reorganization energies

$$\lambda_i^{\text{var}} = \beta \langle (\delta X)^2 \rangle_i / 2 \tag{9}$$

The average here is taken over two fluctuating fields: the scalar field  $\delta\phi_b$  and the second-rank field tensor  $F_b$ . Correspondingly, the Stokes-shift reorganization energy becomes

$$2\lambda^{\text{St}} = e(\langle \phi_{\text{b}} \rangle_{\text{Red}} - \langle \phi_{\text{b}} \rangle_{\text{Ox}}) + \frac{1}{2} \Delta \alpha : [\langle \mathbf{F}_{\text{b}} \rangle_{\text{Red}} - \langle \mathbf{F}_{\text{b}} \rangle_{\text{Ox}}]$$
(10)

These results are shown in Figure 1, where the polarizability matrix  $\Delta \alpha \to \zeta \Delta \alpha$  is scaled with the parameter  $-2 \le \zeta \le 2$  to

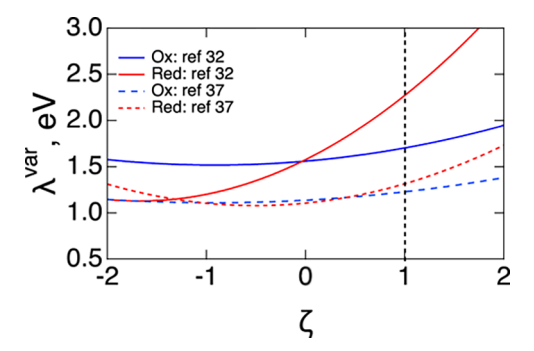


**Figure 1.** Reorganization energies of Ox and Red states calculated from eqs 7 and 8 with anisotropic polarizability  $\Delta\alpha$  given in eq 11. The stochastic fields  $\phi_{\rm b}$ ,  $E_{\rm b}$  are taken from molecular dynamics simulation in refs 32 and 37 as indicated in the plot. The scaling parameter  $\zeta$  scales  $\Delta\alpha$  to  $\Delta\zeta\alpha$  to illustrate the effect of changing the overall polarizability magnitude without altering its anisotropy. The dashed vertical line indicates  $\zeta=1$  corresponding to the reorganization energies listed in Table 2.

investigate the effect of altering the polarizability change on the reorganization energy. In Figure 2, similar results are shown by

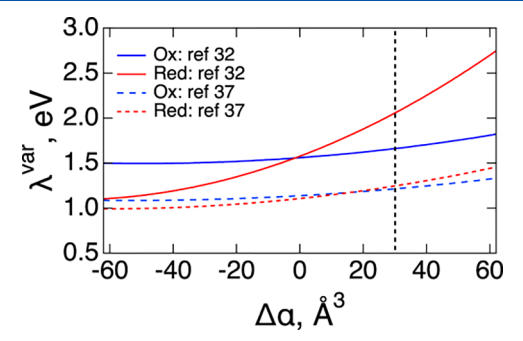


**Figure 2.** Reorganization energies of Ox and Red states calculated from eqs 7 and 8 and isotropic polarizability change  $\Delta \alpha$  according to simulations in refs 32 and 37 (dashed lines).

assuming the isotropic polarizability  $\Delta \alpha^{\alpha\beta} = \Delta \alpha \delta_{\alpha\beta}$ , where  $\Delta \alpha = 31 \text{ Å}^3$  (Table 1). The polarizability tensor is in fact highly anisotropic, which is quantified by a significant difference in the eigenvalues of the polarizability matrix and by the anisotropy parameter  $\gamma$  also listed in Table 1 ( $\gamma$  = 0 for an isotropic polarizability).

The calculations presented in Figures 1 and 2 are based on two sets of stochastic fields,  $\phi_b$  and  $E_b$ , produced in the simulations in refs 32 and 37. The distributions of electrostatic potentials (Figure 3) and field magnitudes (Figure 4) are consistent between these two sets of simulations. The reorganization energies produced are listed, among other results reported in the past, in Table 2. The classical simulations listed in the table are based on assuming that the entire transferred charge is localized on the Fe atom of the heme. This calculation is sufficiently close to the more often implemented summation  $\sum_j \Delta q_j \phi_{bj}$  over changes in partial atomic charges  $\Delta q_j$  within the active site. This result, listed in the second line of Table 2, refers to  $\Delta \alpha = 0$  in eq 8. Enabling  $\Delta \alpha = 31 \text{ Å}^3$  does not strongly affect  $\lambda^{\text{St}}$  but noticeably affects  $\lambda^{\text{var}}_i$  (line 9 in Table 2).

Even the grossly simplified model based on the isotropic polarizability of the active site (Figure 2) qualitatively supports more advanced calculations based on the empirical valence-

The Journal of Physical Chemistry B

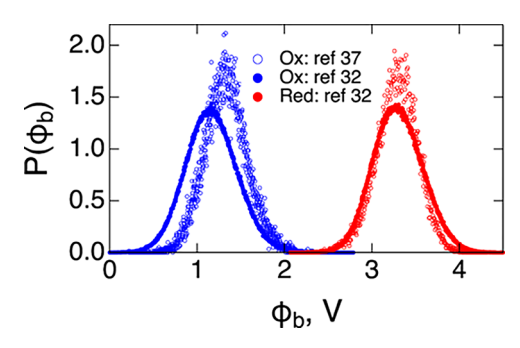
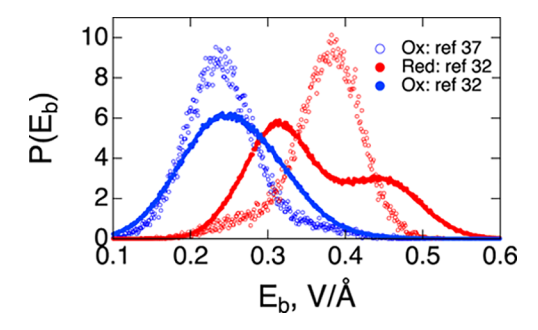


Figure 3. Distribution of the bath electrostatic potential  $\phi_b$  at the Fe atom of the heme calculated for Ox (blue) and Red (red) states from simulation trajectories produced in ref 32 (filled points) and in ref 37 (open points).



**Figure 4.** Distribution of the magnitude of the electrostatic field  $E_{\rm b}$  at the Fe atom of the heme calculated for Ox (blue) and Red (red) states from simulation trajectories produced in ref 32 (filled points) and in ref 37 (open points).

bond diagonalization. The split between two  $\lambda_i^{\rm var}$  and  $\kappa_{\rm G} > 1$  grows with increasing  $\Delta\alpha$ . Of course, the free energy surfaces of electron transfer describing polarizable systems are non-parabolic. However, a simplified description in terms of crossing parabolas with different curvatures is in many cases sufficient for the practical purpose of calculating the activation barrier. In contrast to our calculations shown in Figure 1, ref 37 claims that the electric field needs to be increased by a factor of 5 to reach a significant effect of polarizability on the reorganization energy. This claim is inconsistent with the electrostatic data produced by both simulations (Figures 3 and 4). For instance, when the suggested 5-fold increase of the electric field is applied to the Red state,  $\lambda_{\rm Red}^{\rm var}$  from eqs 8 and 9, calculated with the  $\phi_{\rm b}$ ,  $E_{\rm b}$  from ref 37, becomes equal to 22 eV.

Introducing anisotropic polarizability tensor further increases  $\lambda^{\rm var}$  and  $\kappa_{\rm G}$  (line 11 in Table 2). This anisotropydriven enhancement might be underestimated in our calculations since polarizability is a property slowly converging with the number of states involved and including more excited states might affect the result. Including anisotropic  $\alpha$  further enhances  $\lambda^{\rm var}$  because the asymmetry of the polarizability matrix  $\Delta\alpha$  matches the asymmetry of the electric field tensor  $\langle \mathbf{F}_{\rm b} \rangle$ . We find the following values for  $\Delta\alpha$  (in ų) and  $\langle \mathbf{F}_{\rm b} \rangle$  (in  $(V/\text{Å})^2$ )

Table 2. Reorganization Energies (eV) and the Parameter  $\kappa_G$  (Eq 3) from Different Simulations of Cytochrome c

method	$\lambda^{\mathrm{St}}$	$\lambda_{\mathrm{Ox}}^{\mathrm{var}}$	$\lambda_{ m Red}^{ m var}$	$\kappa_{ m G}$	ref
EVB MD <sup>a</sup>	0.89	0.92	1.32	1.3	33
classical MD <sup>b</sup>	1.13	1.57	1.50	1.3	32
classical MD <sup>c</sup>	0.98	1.14	1.11	1.2	37
EVB MD <sup>d</sup>	$1.20 \pm 0.04$	$3.10 \pm 0.14$	$2.34 \pm 0.09$	2.26	32
EVB MD (no rot, zero dipoles) <sup>e</sup>	$1.08 \pm 0.06$	$1.76 \pm 0.12$	$1.63 \pm 0.11$	1.57	32
EVB MD <sup>f</sup>	$1.00 \pm 0.01$	$1.23 \pm 0.08$	$1.24 \pm 0.07$	1.23	37
EVB MD (no rot, zero dipoles) <sup>e</sup>	$1.00 \pm 0.01$	$1.29 \pm 0.05$	$1.23 \pm 0.06$	1.26	37
EVB MD (no rot) <sup>g</sup>	$0.98 \pm 0.02$	$1.46 \pm 0.08$	$2.67 \pm 0.36$	2.11	37
Isotropic polar	izability				
eq 2 <sup>h</sup>	1.15	1.66	2.07	1.63	32
eq 2 <sup>i</sup>	1.06	1.22	1.25	1.16	37
Anisotropic po	olarizability				
eq 2 <sup>j</sup>	1.17	1.84	2.15	1.70	32
eq 2 <sup>j</sup>	1.06	1.23	1.31	1.19	37

<sup>a</sup>The empirical valence-bond calculations performed in ref 33 involved only 13 states and resulted in nearly zero polarizability. The values listed here are produced from trajectories supplied by the authors of ref 33. <sup>b</sup>Calculated assuming the entire charge is localized on the Fe atom of the heme upon electron transfer. <sup>c</sup>Same calculation as in table note b with  $\phi_{\rm b}$ ,  ${\bf E}_{\rm b}$  from ref 37.  $^d$ All uncertainties reported in this table, except for line 6, are from five blocks along the trajectory calculated as deviations from block averages. eThe electric field was not rotated to the coordinate frame of the quantum center and the diagonal dipoles of the dipole moment matrix were set equal to zero,  $\mu_{jj} = 0.$  Results reported in Table 1 (marked as QM2/SF1) in ref 37. The electric field was not rotated to the coordinate frame of the quantum center, but  $\mu_{ii}$  from our own calculations of the quantum center used in ref 37 were applied to the Hamiltonian matrix in eq 7 (the quantum centers used in refs 32 and 37 are slightly different).  $^{h}$ Calculated from eqs 9 and 10 with the isotropic polarizabilities  $\alpha_{\rm Ox}$  = 23 Å<sup>3</sup> and  $\alpha_{Red}$  = 54 Å<sup>3</sup> (Table 1) and  $\phi_b$ ,  $E_b$  from ref 32. Same calculation as in table note g with  $\phi_{\mathrm{b}}$ ,  $\mathbf{E}_{\mathrm{b}}$  from ref 37.  $^{j}$ Same calculations as in table notes g and h, but with anisotropic polarizability  $\Delta \alpha$  from eq 11.

$$\Delta \alpha = \begin{pmatrix} 16.7 & -19.6 & 2.85 \\ -19.6 & 30.3 & 0.77 \\ 2.85 & 0.77 & 45.2 \end{pmatrix},$$

$$\langle \mathbf{F}_{b} \rangle_{\text{Red}} = \begin{pmatrix} 0.004 & 0 & -0.002 \\ 0 & 0.016 & 0.040 \\ -0.002 & 0.040 & 0.117 \end{pmatrix}$$
(11)

For both tensors,  $\Delta\alpha$  and  $\langle F_b \rangle$ , the largest values are gained for the zz projection in the molecular frame used in our calculations. As shown in the cartoon of the active site in Figure 5, this is the direction in the plane of the heme. The highest polarizability of the active site along the z axis is combined with the highest electric field produced by the medium in this direction. This match, which might be driven by the specific fold of the protein, makes larger the tensor contraction in the second term in eq 8, thus leading to a higher  $\lambda^{\rm var}$ .

The Journal of Physical Chemistry B

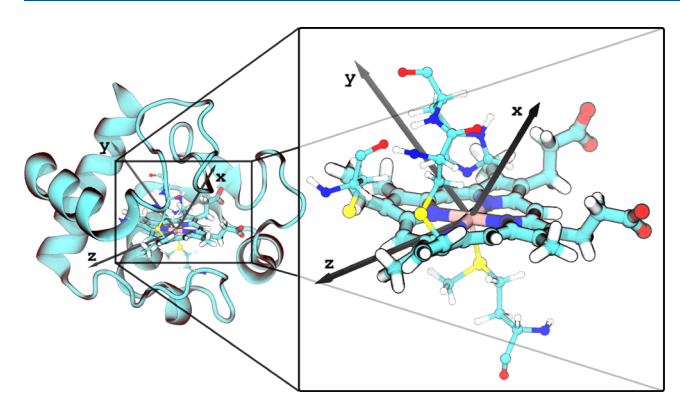


**Figure 5.** Active site in the molecular frame of the quantum calculation.  $^{32}$ 

The anisotropy of  $\mathbf{F}_b$ , which is clearly seen in our calculations, does not appear from the electric field trajectories in ref 37. This is because the authors presumably failed to rotate the vector of the electric field of the protein-water medium  $\mathbf{E}_b$  to the molecular frame of the active site in which the set of diagonal and off-diagonal (transition) dipoles is calculated to be used in the empirical valence-bond diagonalization (eq 7). The electric field tensor  $\mathbf{F}_b$  gets averaged over the rotations of the protein on a sufficiently long trajectory, thus becoming effectively isotropic. We attempted to reproduce this outcome by skipping field rotation and thus allowing the frame of reference to rotate along the simulation trajectory. The field tensor  $((V/\text{Å})^2)$  becomes much more isotropic compared to the one shown in eq 11

$$\langle \mathbf{F}_{b} \rangle_{\text{Red}} = \begin{pmatrix} 0.031 & 0.007 & 0.001 \\ 0.007 & 0.064 & -0.002 \\ 0.001 & -0.002 & 0.044 \end{pmatrix}$$
 (12)

This symmetry is similar to what we find from the results presented in ref 37. This calculation error is responsible for a weak effect of the polarizability anisotropy on the reorganization energy  $\lambda^{\text{var}}$  (Figures 1 and 2 and Table 2). To estimate the effect of neglecting frame rotation on the empirical valence-bond diagonalization, we compared our previous calculations with rotations involved (line 4 in Table 2) with the same calculations when no rotations were performed (line 5 in Table 2). The result is a much lower  $\kappa_{\text{G}}$ , although not as low as reported in ref 37 (line 6).

Another and more significant distinction of the calculations performed in ref 37 from ours, leading to erroneous results, is the neglect of diagonal dipole moments in the Hamiltonian matrix ( $\mu_{jj}$  in eq 7). Since the standard Gaussian output does not list dipole moments of the excited states, a separate calculation for each excited state was carried out in our study.<sup>32</sup> We could reproduce the results from Table 1 in ref 37 (labeled as QM2/SF1) by performing calculations with the matrix of nonzero off-diagonal transition dipoles and zero diagonal dipoles ( $\mu_{jj} = 0$ ) combined with the trajectories of the electrostatic potential and field from their simulations (cf. lines 6 and 7 in Table 2).

The omission of the diagonal dipoles effectively eliminates modulation of the active site polarizability by the field, that is, all higher-order polarizabilities. To confirm these results, we additionally used the definition of the quantum center from ref 37 to calculate the diagonal dipole moments in the Hamiltonian matrix (listed in the Supporting Information)

and reran the calculations using their trajectories of fields and potentials (line 8 in Table 2). Since no rotations of the fields to the frame of the quantum center were performed in their calculations, the results are still incorrect. However, the reorganization energies  $\lambda^{var}$  are significantly shifted upward and the resulting  $\kappa_G = 2.11$  becomes much closer to our result  $\kappa_{\rm G}$  = 2.26. From two calculation errors in ref 37, the omission of field rotations and the neglect of the diagonal dipole moments, the second one appears to be most severe. We note that the interaction of the diagonal dipole with the proteinwater electric field is significant. For instance, one gets the following values for the interaction energy  $\mu_{11}^i \langle E_b \rangle$  of the ground-state dipole with the average electrostatic field: 3.1 (i =Ox) and 4.3 eV (i = Red). These numbers should be compared with the vacuum energy gaps between the first excited and ground states  $E_2^i - E_1^i$  amounting to 0.33 eV (Ox) and 0.84 eV (Red).

#### DISCUSSION

A close match in asymmetries between the polarizability difference tensor  $\Delta\alpha$  and the electric field tensor  $\langle F_b\rangle$  suggests a potential reason for the specific design of the active sites of cytochromes. The heme is inserted in the protein pocket and remains open to water only from one side. In this way, the direction of the highest polarizability, in the heme's plane, coincides with the direction of the highest potential gradient from the heme toward water. The electric field ensured by this potential gradient couples to the polarizability change in the heme's plane to increase both the reorganization energy  $\lambda^{\rm var}$  and  $\kappa_{\rm G}$ . The barrier of the reaction is lowered (eq 5) and the catalytic effect is achieved.

Our calculations confirm this hypothesis. We find that  $\langle F_b \rangle$  arising from the protein matrix is nearly symmetric. All asymmetry of the field tensor in eq 11 arises from the water component of the thermal bath. As a result, the reorganization energies  $\lambda_i^{\text{var}}$  calculated in eqs 8 and 9 from water only are equal to 3.5 eV (Ox) and 2.8 eV (Red). As shown in Table 2 (line 11), the total reorganization energies are 1.84 and 2.15 eV. This result implies that cross-correlations between the protein and water electrostatic fluctuations, accounting for the screening of the water fluctuations by the protein-water interface, produce negative contributions exceeding in magnitude the reorganization energies from the protein, 3.2 eV (Ox) and 2.5 eV (Red).

The variance of the electron-transfer energy gap  $\sigma^2(T)$ shows a behavior more complex than the linear scaling,  $\sigma^2(T)$  $\propto T$ , predicted by the fluctuation–dissipation theorem.<sup>53</sup> Instead, a crossover with lowering temperature has been observed for all proteins for which this function was studied by simulations.<sup>31</sup> The crossover occurs in the range of temperatures  $\sim$ 200 K consistent with the temperature of the dynamical transition in proteins. Specifically, the variance has a steeper slope at higher temperatures scaling as  $\sigma^2 \propto (T T_0$ ). It turns to a linear scaling consistent with the fluctuation dissipation theorem below the dynamical transition. Figure 6 shows that plastocyanin (half reaction) and a green fluorescent protein (intraprotein electron transfer) obey this phenomenology also found for many glassy media. 31,32 The result of this specific temperature scaling is that the rate constant of electron transfer is expected to follow the Vogel-Fulcher law instead of the Arrhenius law. 27,31

The temperature variation of  $\sigma^2(T)$  for cytochrome  $c^{56}$  is distinctly different from other electron-transfer proteins

The Journal of Physical Chemistry B

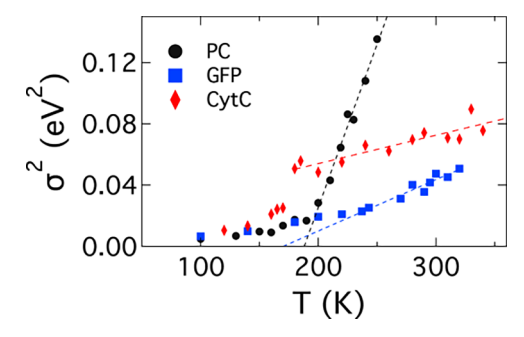


**Figure 6.** Temperature dependence of  $\sigma^2 = \langle (\delta X)^2 \rangle$  for plastocyanin (PC, half reaction), green fluorescent protein (GFP, intraprotein electron transfer), and Ox cytochrome c (CytC, half reaction). The dashed lines are linear fits of high-temperature portions of  $\sigma^2(T)$ .

studied by simulations. The variance and the reorganization energy  $\lambda^{\text{var}}$  drop at the temperature more consistent with the temperature  $T_{\rm g}$  of glass transition of proteins.<sup>57</sup> The drop of  $\sigma^2$ at  $T_g$  is not in the form of breaking the linear slope but is more consistent with the standard ergodicity breaking (dynamical freezing) found in bulk glass formers at the glass transition.<sup>40</sup> This change in the temperature law is yet another indication of distinct statistics of fluctuations observed for proteins displaying nonergodic sampling and cytochrome c. While  $\kappa_G$ for the former is linked to insufficient exploration of configuration space,  $\kappa_G > 1$  for cytochrome c is caused by a relatively high polarizability of its active site. This high polarizability was not realized in our simulations of the chain of iron-sulfur clusters in the bacterial complex I.30 The mechanism behind  $\kappa_G > 1$  in that system was a combination of nonergodic sampling with partial wetting of the active sites along the electron transport path. All these differences disappear at low temperatures below the temperature of dynamical/glass transition. The variance reorganization energy at low temperatures is caused by fast localized motions of charged and polar groups near equilibrium positions, and the resulting reorganization energies are roughly consistent among different proteins (Figure 6).

The temperature dependence of the reorganization energy deserves a separate comment. Experiments show that  $\lambda^{\rm r}$  extracted from electrochemistry of surface-immobilized myoglobin is little sensitive to temperature. On the contrary,  $\lambda$  of the standard Marcus formulation, carrying the meaning of the free energy of solvating the electron-transfer dipole, noticeably decays with increasing temperature. If one defines the entropy

$$S_{\lambda} = -(\partial \lambda / \partial T)_{p} \tag{13}$$

then  $TS_{\lambda}/\lambda \simeq 0.5$  is typically found for electron-transfer reactions involving organic donor—acceptor systems. On the contrary, the composite reorganization energy  $\lambda^{\rm r}$  in eq 4 varies with temperature based on two separate entropies,  $S_{\lambda}^{\rm St}$  and  $S_{\lambda}^{\rm var}$ ,

$$S_{\lambda}^{r} = \kappa_{G}^{-2} [2\kappa_{G} S_{\lambda}^{St} - S_{\lambda}^{var}] \tag{14}$$

As the result of compensation between  $S_{\lambda}^{\rm St} > 0$  and  $S_{\lambda}^{\rm var} > 0$  in the brackets in this equation,  $S_{\lambda}^{\rm r}$  is about an order of magnitude smaller than  $S_{\lambda}^{\rm var}$ : one gets  $TS_{\lambda}/\lambda \simeq 0.25$  in this case. The composite reaction reorganization energy  $\lambda^{\rm r}$  not only lowers the activation barrier but also results in a robust operation of the enzyme weakly affected by temperature. The observation of low temperature sensitivity of the reorganization energy in experiment and its realization in simulations gives

additional support to the composite form of the observable  $\lambda^r$  given by eq 4.

The new analysis of the reorganization energy of cytochrome c by a number of simulation protocols presented in ref 37 suggests that recently developed polarizable force fields for protein and water<sup>58,59</sup> produce better quantitive agreement with published experimental reorganization energies compared to nonpolarizable force fields. A direct comparison between two sets of force fields for electron-transfer energetics is still a challenging task since reduction of the system size and lower statistics are still required to implement more demanding polarizable force fields.<sup>37,60</sup> It is also clear that success of polarizable models in the homogeneous environment of the bulk, where mean-field models are very successful, 61 does not necessarily project to heterogenous interfaces and solvation.<sup>62</sup> The problem needs further studies from the fundamental perspective since increasing solvent polarizability at constant permanent dipole in model polarizable fluids produces a weaker effect of polarizability on the reorganization energy than predicted by the Pekar factor. 63,64 The distinction between medium reorganization for protein electron transfer from other systems is a strong compensation,<sup>29</sup> mentioned above, between the protein and water reorganization components in the total  $\lambda^{\text{var}}$ . The details of the cross protein-water correlations of electrostatic fluctuations in the protein-water interface need to be adequately reproduced by the polarizable force field. From the viewpoint of comparison to experiment, collecting sufficient statistics from long trajectories with the standard nonpolarizable force fields was sufficient to achieve quantitative agreement with published kinetic data for fast electron transfer in bacterial reaction centers. 17,26

## CONCLUSIONS

We emphasize here that redox proteins offer a number of potentially important mechanisms for achieving the catalytic effect, alongside with the traditional mechanism of reaching the activation barrier through collective polarization fluctuations of the polarizable medium.<sup>2</sup> Nonergodic sampling and penetration of water to the protein's core are the mechanisms specific to proteins. The difference in polarizabilities of Ox and Red states is a more general mechanism applicable to all electron-transfer reactions, which gains importance depending on the magnitude of the polarizability change between the oxidation states.

Cytochrome c is an important case of a protein for which nonergodic sampling found in simulations of many other proteins was not reproduced. To explain reorganization energies reported by electrochemistry, polarizability of the active site was included. It results in a depression of the activation barrier similar to the effect of nonergodicity, as indeed confirmed by calculations based on the empirical valence-bond method.<sup>32</sup> These results were recently challenged in ref 37, which could not confirm our previous reports. In an attempt to test different simulation/calculation protocols, a direct formalism for calculating the reorganization parameters from anisotropic linear polarizability and electrostatics produced by simulations is introduced here. Our present calculations confirm that polarizability of the active site couples to high-magnitude fluctuations of electrostatic fields and potentials from the protein-water interface to produce a significant depression of the electron-transfer activation barrier. This simplified model qualitatively supports previous findings involving full diagonalization of the active-site Hamiltonian and points to the deficiencies of the analysis attempted in ref 37. More importantly, it provides a transparent and physically appealing approach to study protein electron transfer involving polarizable active sites.

We find a curious match between the anisotropies of the polarizability difference tensor and the tensor of the electric field produced by the protein-water thermal bath. It appears that the design of cytochrome's active site allows large electric fields, originating from the contact between the heme and water, along the heme's plane where the active site is most polarizable. There are a number of instances found in previous simulations where partial penetration of water into the active site is significant for the electron-transfer kinetics<sup>30,51</sup> and for other protein function.<sup>33,65–67</sup> The general design principle in all such cases is the creation of strong interfacial heterogeneity and related strong interfacial electric fields. Here, we find that such fields, induced by the protein-water interface, combine with anisotropic polarizability of the active site to allow the depression of the activation barrier.

#### ASSOCIATED CONTENT

## S Supporting Information

The Supporting Information is available free of charge at https://pubs.acs.org/doi/10.1021/acs.jpcb.9b09236.

Diagonal elements of the dipolar matrix calculated for the active site as defined in refs 32 and 37 (PDF)

## AUTHOR INFORMATION

## **Corresponding Author**

\*E-mail: dmitrym@asu.edu. Tel: (480)965-0057.

# ORCID ®

Dmitry V. Matyushov: 0000-0002-9352-764X

## Notes

The authors declare no competing financial interest.

#### ACKNOWLEDGMENTS

This research was supported by the National Science Foundation (CHE-1800243). The authors are grateful to Jochen Blumberger for providing electrostatic data and results of quantum calculations from ref 37.

#### REFERENCES

- (1) Pauling, L. Molecular architecture and biological reactions. Chem. Eng. News 1946, 24, 1375–1377.
- (2) Marcus, R. A.; Sutin, N. Electron transfer in chemistry and biology. *Biochim. Biophys. Acta* **1985**, *811*, 265–322.
- (3) Bard, A. J.; Faulkner, L. R. Electrochemical Methods. Fundamentals and Applications, 2nd ed.; Wiley: New York, 2001.
- (4) Gray, H. B.; Winkler, J. R. Electron tunneling through proteins. Q. Rev. Biophys. **2003**, 36, 341–372.
- (5) Cheng, J.; Terrettaz, S.; Blankman, J. I.; Miller, C. J.; Dangi, B.; Guiles, R. D. Electrochemical comparison of heme proteins by insulated electrode voltammetry. *Isr. J. Chem.* **1997**, *37*, 259–266.
- (6) Wei, J. J.; Liu, H.; Niki, K.; Margoliash, E.; Waldeck, D. H. Probing Electron Tunneling Pathways: Electrochemical Study of Rat Heart Cytochrome c and Its Mutant on Pyridine-Terminated SAMs. *J. Phys. Chem. B* **2004**, *108*, 16912–16917.
- (7) Khoshtariya, D. E.; Dolidze, T. D.; Shushanyan, M.; van Eldik, R. Long-range electron transfer with myoglobin immobilized at Au/mixed-SAM junctions: Mechanistic impact of the strong protein confinement. J. Phys. Chem. B 2014, 118, 692–706.

- (8) Khoshtariya, D. E.; Dolidze, T. D.; Shushanyan, M.; Davis, K. L.; Waldeck, D. H.; van Eldik, R. Fundamental signatures of short- and long-range electron transfer for the blue copper protein azurin at Au/SAM junctions. *Proc. Natl. Acad. Sci. U. S. A.* **2010**, *107*, 2757.
- (9) Monari, S.; Battistuzzi, G.; Bortolotti, C. A.; Yanagisawa, S.; Sato, K.; Li, C.; Salard, I.; Kostrz, D.; Borsari, M.; Ranieri, A.; et al. Understanding the mechanism of short-range electron transfer using an immobilized cupredoxin. *J. Am. Chem. Soc.* **2012**, *134*, 11848–11851
- (10) Jeuken, L. J. C.; McEvoy, J. P.; Armstrong, F. A. Insights into gated electron-transfer kinetics at the electrode-protein interface: A square wave voltammetry study of the blue copper protein azurin. *J. Phys. Chem. B* **2002**, *106*, 2304.
- (11) Guo, Y.; Zhao, J.; Yin, X.; Gao, X.; Tian, Y. Electrochemistry Investigation on Protein Protection by Alkanethiol Self-Assembled Monolayers against Urea Impact. *J. Phys. Chem. C* **2008**, *112*, 6013–6021.
- (12) Ghorai, P. K.; Matyushov, D. V. Solvent reorganization entropy of electron transfer in polar solvents. *J. Phys. Chem. A* **2006**, *110*, 8857–8863.
- (13) Mines, G. A.; Bjerrum, M. J.; Hill, M. G.; Casimiro, D. R.; Chang, I.-J.; Winkler, J. R.; Gray, H. B. Rates of Heme Oxidation and Reduction in Ru(His33)cytochrome c at Very High Driving Forces. *J. Am. Chem. Soc.* **1996**, *118*, 1961–1965.
- (14) Farver, O.; Hosseinzadeh, P.; Marshall, N. M.; Wherland, S.; Lu, Y.; Pecht, I. Long-range electron transfer in engineered azurins exhibits Marcus inverted region behavior. *J. Phys. Chem. Lett.* **2014**, *6*, 100–105.
- (15) Blumberger, J. Free energies for biological electron transfer from QM/MM calculation: method, application and critical assessment. *Phys. Chem. Chem. Phys.* **2008**, *10*, 5651–5667.
- (16) McCullagh, M.; Voth, G. A. Unraveling the Role of the Protein Environment for [FeFe]-Hydrogenase: A New Application of Coarse-Graining. *J. Phys. Chem. B* **2013**, *117*, 4062–4071.
- (17) LeBard, D. N.; Martin, D. R.; Lin, S.; Woodbury, N. W.; Matyushov, D. V. Protein dynamics to optimize and control bacterial photosynthesis. *Chem. Sci.* **2013**, *4*, 4127–4136.
- (18) Tan, C.; Liu, Z.; Li, J.; Guo, X.; Wang, L.; Sancar, A.; Zhong, D. The molecular origin of high DNA-repair efficiency by photolyase. *Nat. Commun.* **2015**, *6*, 7302.
- (19) Liu, Z.; Guo, X.; Tan, C.; Li, J.; Kao, Y.-T.; Wang, L.; Sancar, A.; Zhong, D. Electron tunneling pathways and role of adenine in repair of cyclobutane pyrimidine dimer by DNA photolyase. *J. Am. Chem. Soc.* **2012**, *134*, 8104–8114.
- (20) Sigfriddson, E.; Olsson, M. H. M.; Ryde, U. A comparison of the inner-sphere reorganization energies of cytochromes, iron—sulfur clusters, and blue copper proteins. *J. Phys. Chem. B* **2001**, *105*, 5546—5552
- (21) Warshel, A. Dynamics of reactions in polar solvents. Semiclassical trajectory studies of electron-transfer and proton-transfer reactions. *J. Phys. Chem.* **1982**, *86*, 2218–2224.
- (22) Kuharski, R. A.; Bader, J. S.; Chandler, D.; Sprik, M.; Klein, M. L.; Impey, R. W. Molecular model for aqueous ferrous-ferric electron transfer. *J. Chem. Phys.* **1988**, *89*, 3248–3257.
- (23) Matyushov, D. V.; Voth, G. A. Modeling the free energy surfaces of electron transfer in condensed phases. *J. Chem. Phys.* **2000**, 113, 5413.
- (24) Matyushov, D. V. Protein electron transfer: Dynamics and statistics. *J. Chem. Phys.* **2013**, *139*, No. 025102.
- (25) LeBard, D. N.; Matyushov, D. V. Glassy protein dynamics and gigantic solvent reorganization energy of plastocyanin. *J. Phys. Chem. B* **2008**, *112*, 5218–5227.
- (26) LeBard, D. N.; Kapko, V.; Matyushov, D. V. Energetics and kinetics of primary charge separation in bacterial photosynthesis. *J. Phys. Chem. B* **2008**, *112*, 10322–10342.
- (27) Martin, D. R.; Matyushov, D. V. Non-Gaussian statistics and nanosecond dynamics of electrostatic fluctuations affecting optical transitions in a green fluorescent protein. *J. Phys. Chem. B* **2012**, *116*, 10294–10300.

- (28) Martin, D. R.; LeBard, D. N.; Matyushov, D. V. Coulomb soup of bioenergetics: Electron transfer in a bacterial bc1 complex. *J. Phys. Chem. Lett.* **2013**, *4*, 3602–3606.
- (29) Martin, D. R.; Matyushov, D. V. Communication: Microsecond dynamics of the protein and water affect electron transfer in a bacterial bc1 complex. *J. Chem. Phys.* **2015**, *142*, 161101.
- (30) Martin, D. R.; Matyushov, D. V. Electron-transfer chain in respiratory complex I. Sci. Rep. 2017, 7, 5495.
- (31) Matyushov, D. V. Protein electron transfer: is biology (thermo)dynamic? *J. Phys.: Condens. Matter* **2015**, *27*, 473001.
- (32) Dinpajooh, M.; Martin, D. R.; Matyushov, D. V. Polarizability of the active site of cytochrome *c* reduces the activation barrier for electron transfer. *Sci. Rep.* **2016**, *6*, 28152.
- (33) Bortolotti, C. A.; Amadei, A.; Aschi, M.; Borsari, M.; Corni, S.; Sola, M.; Daidone, I. The reversible opening of water channels in cytochrome c modulates the heme iron reduction potential. *J. Am. Chem. Soc.* **2012**, *134*, 13670–13678.
- (34) Warshel, A.; Bora, R. P. Perspective: Defining and quantifying the role of dynamics in enzyme catalysis. *J. Chem. Phys.* **2016**, *144*, 180901.
- (35) Daidone, I.; Amadei, A.; Zaccanti, F.; Borsari, M.; Bortolotti, C. A. How the reorganization free energy affects the reduction potential of structurally homologous cytochromes. *J. Phys. Chem. Lett.* **2014**, *5*, 1534–1540.
- (36) Seyedi, S. S.; Waskasi, M. M.; Matyushov, D. V. Theory and electrochemistry of cytochrome c. J. Phys. Chem. B **2017**, 121, 4958–4967.
- (37) Jiang, X.; Futera, Z.; Blumberger, J. Ergodicity-breaking in thermal biological electron transfer? Cytochrome *c* revisited. *J. Phys. Chem. B* **2019**, *123*, 7588–7598.
- (38) Blumberger, J. Recent advances in the theory and molecular simulation of biological electron transfer reactions. *Chem. Rev.* **2015**, *115*, 11191–11238.
- (39) Stillinger, F. H. Energy Landscapes, Inherent Structures, and Condensed-Matter Phenomena; Princeton University Press: Princeton, NI. 2016
- (40) Angell, C. A. Formation of glasses from liquids and biopolymers. *Science* **1995**, *267*, 1924–1935.
- (41) Frauenfelder, H.; Sligar, S. G.; Wolynes, P. G. The energy landscapes and motions of proteins. *Science* **1991**, *254*, 1598–1603.
- (42) Frauenfelder, H.; Chen, G.; Berendzen, J.; Fenimore, P. W.; Jansson, H.; McMahon, B. H.; Stroe, I. R.; Swenson, J.; Young, R. D. A unified model of protein dynamics. *Proc. Natl. Acad. Sci. U. S. A.* **2009**, *106*, 5129–5134.
- (43) Min, W.; English, B. P.; Luo, G.; Cherayil, B. J.; Kou, S. C.; Xie, X. S. Fluctuating enzymes: Lessons from single-molecule studies. *Acc. Chem. Res.* **2005**, *38*, 923–931.
- (44) Iversen, L.; Tu, H.-L.; Lin, W.-C.; Christensen, S. M.; Abel, S. M.; Iwig, J.; Wu, H.-J.; Gureasko, J.; Rhodes, C.; Petit, R. S.; et al. Ras activation by SOS: Allosteric regulation by altered fluctuation dynamics. *Science* **2014**, 345, 50–54.
- (45) Shepard, W. E. B.; Anderson, B. F.; Lewandoski, D. A.; Norris, G. E.; Baker, E. N. Copper coordination geometry in azurin undergoes minimal change on reduction of copper(II) to copper(I). *J. Am. Chem. Soc.* **1990**, *112*, 7817–7819.
- (46) Li, Z.; Raychaudhuri, S.; Wand, A. J. Insights into the local residual entropy of proteins provided by NMR relaxation. *Protein Sci.* **1996**, *5*, 2647–2650.
- (47) Cascella, M.; Magistrato, A.; Tavernelli, I.; Carloni, P.; Rothlisberger, U. Role of protein frame and solvent for the redox properties of azurin from Pseudomonas aeruginosa. *Proc. Natl. Acad. Sci. U. S. A.* **2006**, *103*, 19641–19646.
- (48) Winkler, J. R.; Gray, H. B. Electron flow through metalloproteins. *Chem. Rev.* **2014**, *114*, 3369–3380.
- (49) Jha, S. K.; Ji, M.; Gaffney, K. J.; Boxer, S. G. Direct measurement of the protein response to an electrostatic perturbation that mimics the catalytic cycle in ketosteroid isomerase. *Proc. Natl. Acad. Sci. U. S. A.* **2011**, *108*, 16612–16617.

- (50) Rahaman, O.; Kalimeri, M.; Melchionna, S.; Hénin, J.; Sterpone, F. Role of internal water on protein thermal stability: The case of homologous G domains. *J. Phys. Chem. B* **2015**, *119*, 8939–8949.
- (51) Martin, D. R.; Matyushov, D. V. Photosynthetic diode: Electron transport rectification by wetting the quinone cofactor. *Phys. Chem. Phys.* **2015**, *17*, 22523–22528.
- (52) Waskasi, M. M.; Martin, D. R.; Matyushov, D. V. Wetting of the protein active site leads to non-Marcusian reaction kinetics. *J. Phys. Chem. B* **2018**, *122*, 10490–10495.
- (53) Kubo, R. The fluctuation-dissipation theorem. Rep. Prog. Phys. 1966, 29, 255–284.
- (54) Parak, F. G. Physical aspects of protein dynamics. Rep. Prog. Phys. 2003, 66, 103–129.
- (55) Doster, W. The protein-solvent glass transition. *Biochim. Biophys. Acta* **2010**, *1804*, 3–14.
- (56) Seyedi, S.; Matyushov, D. V. Termination of biological function at low temperatures: Glass or structural transition? *J. Phys. Chem. Lett.* **2018**, *9*, 2359–2366.
- (57) Khodadadi, S.; Malkovskiy, A.; Kisliuk, A.; Sokolov, A. P. A broad glass transition in hydrated proteins. *Biochim. Biophys. Acta* **2010**, *1804*, 15–19.
- (58) Lemkul, J. A.; Huang, J.; Roux, B.; MacKerell, A. D., Jr. An empirical polarizable force field based on the classical Drude oscillator model: Development history and recent applications. *Chem. Rev.* **2016**, *116*, 4983–5013.
- (59) Cieplak, P.; Dupradeau, F.-Y.; Duan, Y.; Wang, J. Polarization effects in molecular mechanical force fields. *J. Phys.: Condens. Matter* **2009**, *21*, 333102.
- (60) Vladimirov, E.; Ivanova, A.; Rósch, N. Solvent reorganization energies in A-DNA, B-DNA, and rhodamine 6G–DNA complexes from molecular dynamics simulations with a polarizable force field. *J. Phys. Chem. B* **2009**, *113*, 4425–4434.
- (61) Stell, G.; Patey, G. N.; Høye, J. S. Dielectric constants of fluid models: Statistical mechanical theory and its quantitative implementation. *Adv. Chem. Phys.* **1981**, *48*, 183–328.
- (62) Warshel, A.; Kato, M.; Pisliakov, A. V. Polarizable force fields: History, test cases, and prospects. *J. Chem. Theory Comput.* **2007**, *3*, 2034–2045.
- (63) Gupta, S.; Matyushov, D. V. Effects of solvent and solute polarizability on the reorganization energy of electron transfer. *J. Phys. Chem. A* **2004**, *108*, 2087–2096.
- (64) Dinpajooh, M.; Newton, M. D.; Matyushov, D. V. Free energy functionals for polarization fluctuations: Pekar factor revisited. *J. Chem. Phys.* **2017**, *146*, No. 064504.
- (65) Rasaiah, J. C.; Garde, S.; Hummer, G. Water in nonpolar confinement: From nanotubes to proteins and beyond. *Annu. Rev. Phys. Chem.* **2008**, *59*, 713–740.
- (66) Chakrabarty, S.; Warshel, A. Capturing the energetics of water insertion in biological systems: The water flooding approach. *Proteins* **2013**, *81*, 93–106.
- (67) Leioatts, N.; Mertz, B.; Martínez-Mayorga, K.; Romo, T. D.; Pitman, M. C.; Feller, S. E.; Grossfield, A.; Brown, M. F. Retinal ligand mobility explains internal hydration and reconciles active rhodopsin structures. *Biochemistry* **2014**, *53*, 376–385.